Available online at www.sciencedirect.com
SCIENCE DIRECT
Journal of Solid State Chemistry 179 (2006) 2698–2706
JOURNAL OF SOLID STATE CHEMISTRY
www.elsevier.com/locate/jssc

Fabrication and optical properties of core–shell structured spherical SiO_2@$GdVO_4$:Eu^{3+} phosphors via sol–gel process

Guangzhi Li[a,b], Zhenling Wang[a], Min Yu[a,b], Zewei Quan[a], Jun Lin[a,*]

[a]*Key laboratory of Rare Earth Chemistry and Physics, Changchun Institute of Applied Chemistry, Chinese Academy of Sciences, Changchun 130022, PR China*

[b]*Department of Chemistry, Northeast Normal University, Changchun 130024, PR China*

Received 21 April 2006; accepted 7 May 2006
Available online 27 May 2006

Abstract

Europium-doped nanocrystalline $GdVO_4$ phosphor layers were coated on the surface of preformed submicron silica spheres by sol–gel method. The resulted SiO_2@$Gd_{0.95}Eu_{0.05}VO_4$ core–shell particles were characterized by X-ray diffraction (XRD), Fourier transform infrared spectroscopy (FT-IR), scanning electron microscopy (FESEM), energy-dispersive X-ray spectra (EDS), transmission electron microscopy (TEM), photoluminescence (PL) spectra, low voltage cathodoluminescence (CL), time resolved PL spectra and kinetic decays. The XRD results demonstrate that the $Gd_{0.95}Eu_{0.05}VO_4$ layers begin to crystallize on the SiO_2 spheres after annealing at 600 °C and the crystallinity increases with raising the annealing temperature. The obtained core-shell phosphors have spherical shape, narrow size distribution (average size ca. 600 nm), non-agglomeration. The thickness of the $Gd_{0.95}Eu_{0.05}VO_4$ shells on the SiO_2 cores could be easily tailored by varying the number of deposition cycles (50 nm for four deposition cycles). PL and CL show that the emissions are dominated by $^5D_0$–$^7F_2$ transition of Eu^{3+} (618 nm, red). The PL and CL intensities of Eu^{3+} increase with increasing the annealing temperature and the number of coating cycles. The optimum concentration for Eu^{3+} was determined to be 5 mol% of Gd^{3+} in $GdVO_4$ host.

Keywords: SiO_2; $GdVO_4$:Eu^{3+}; Core-shell; Sol–gel process; Luminescent properties

1. Introduction

The surface coating of nanoparticles with various materials to form core–shell morphologies results in the formation of new materials that can be used in the areas of magnetic, mechanical, thermal, electro-optical, electronics, photonics, catalysis, etc. [1–8]. The core–shell materials consist of a core structural domain covered by a shell domain. The core and shell domains may be composed of a variety of materials including polymers, inorganic solids, and metals. Silica coated with other materials are classic materials widely used in many fields of colloid and materials science. Several investigators have reported on the deposition of nanoparticles on silica spheres. They used a variety of techniques including the inverse micelle method, pretreatment steps in electroless plating, double-jet precipitation, layer-by-layer technique, template directed self-assembly and encapsulation of silica nanoparticles by in situ polymerization [9–12]. Generally, these techniques need expensive and complicated equipment setups. There are few literatures reported on silica spheres coated with phosphor layers [13–16]. These core–shell structural phosphors have many merits. First, silica can be easily made controllably in spherical morphology from nano- to micron size [17]. If the silica spheres are coated with layers of phosphors, a kind of core–shell phosphor materials with spherical morphology will be obtained, and the size for the phosphor particles can be controlled by the silica cores. Secondly, the nonagglomeration, narrow size distribution and perfect spherical shape are the ideal morphology of phosphor particles, which has high packing densities and low scattering of light and is good for improvement of brightness and resolution. Finally, because silica is cheaper

*Corresponding author. Tel.: +86 431 5262031; fax: +86 431 5698041.
E-mail address: jlin@ciac.jl.cn (J. Lin).

0022-4596/$ - see front matter © 2006 Elsevier Inc. All rights reserved.
doi:10.1016/j.jssc.2006.05.019

than most of the phosphor materials (which often employ the expensive rare-earth elements as the activators and/or host components), the core–shell phosphor materials will be cheaper than the pure phosphor materials in unit mass.

As laser crystals, $GdVO_4$:RE^{3+} (such as Pr^{3+}, Nd^{3+}, Ho^{3+}, Er^{3+}, Tm^{3+}, Yb^{3+}) have been extensively investigated [18–21]. Although $GdVO_4$:Eu^{3+} will not be used in laser operations, it is excellent red-emitting materials that can be applied in many fields, such as, cathode ray tubes, lamps, X-ray detectors. The luminescence intensity of $GdVO_4$:Eu^{3+} is in the same order as that of YVO_4:Eu^{3+} [22]. In the fields of luminescent material, phosphors based on gadolinium compounds also play an important role because the Gd^{3+} ion ($4f^7$,^8S) has its lowest excited levels at relatively high energy, which is due to the stability of the half-filled shell ground state [23,24]. The luminescence of Eu^{3+} can be sensitized by Gd^{3+}. Therefore, in this paper, we report a simple and economical solution method based on Pechini-type sol–gel process to synthesize the SiO_2@$GdVO_4$:Eu^{3+} core–shell structural phosphors [25]. The structure, morphology and photoluminescent properties of the obtained phosphors were also characterized and discussed in detail.

2. Experimental

2.1. Synthesis of silica cores

Amorphous submicron spheres of silica in the size range of 500–600 nm were synthesized by base-catalyzed hydrolysis of tetraethoxysilane (TEOS) via the well-known Stöber process, i.e., the hydrolysis of TEOS in an ethanol solution containing water and ammonia [26]. This method yielded the colloidal solution of silica particles with a narrow size distribution in submicron range, and the particle size of silica depended on relative concentration of the reactants. In a typical experiment, the mixture containing 0.1 mol/L TEOS (99 wt%, analytical reagent, A.R.), 1 mol/L H_2O, and 7 mol/L NH_4OH (25 wt%, A.R.) was stirred at room temperature (RT) for 4 h, resulting in the formation of white silica colloidal suspension. The silica particles were centrifugally separated from the suspension and washed with ethanol four times.

2.2. Coating of SiO_2 cores with $GdVO_4$:Eu^{3+} shells

SiO_2 core–$GdVO_4$:Eu^{3+} shell particles (SiO_2@$GdVO_4$:Eu^{3+}) were prepared by a sol–gel process [15]. The doping concentrations of Eu^{3+} were 1–11 mol% that of Gd^{3+} in $GdVO_4$:Eu^{3+} host. Stoichiometric amount of Gd_2O_3 (99.99%), Eu_2O_3 (99.99%), was dissolved in dilute HNO_3 (A.R.), under vigorous stirring, and the pH value of the solution was kept between two and three. Then a suitable amount of water–ethanol (v/v = 1:5) solution and stoichiometric amount of ammonium vanadium oxide (NH_4VO_3) was added to the solution. Citric acid (A.R.) was added to the above solution as chelating agent for the metal ions. The molar ratio of metal ions to citric acid was 1:2. Certain amount of polyethylene glycol (PEG, molecular weight = 10 000, A.R.) was added as cross-linking agent. Transparent and blue sols were obtained after stirring for a few hours, and then the as prepared fresh silica particles (without high temperature annealing) were added under stirring. The suspension was further stirred for another 3 h, and then the silica particles were separated by centrifugation. The samples were dried at 100 °C for 1 h and then annealed to the desired temperature (400–1000 °C) with a heating rate of 1 °C/min and held there for 2 h in air. The above process was repeated for several times to increase the thickness of the $GdVO_4$:Eu^{3+} shells. In this way, the core–shell structured SiO_2@$GdVO_4$:Eu^{3+} materials have been obtained, and the whole process is shown in Scheme 1. For the purpose of comparison, the coating sol was evaporated to form

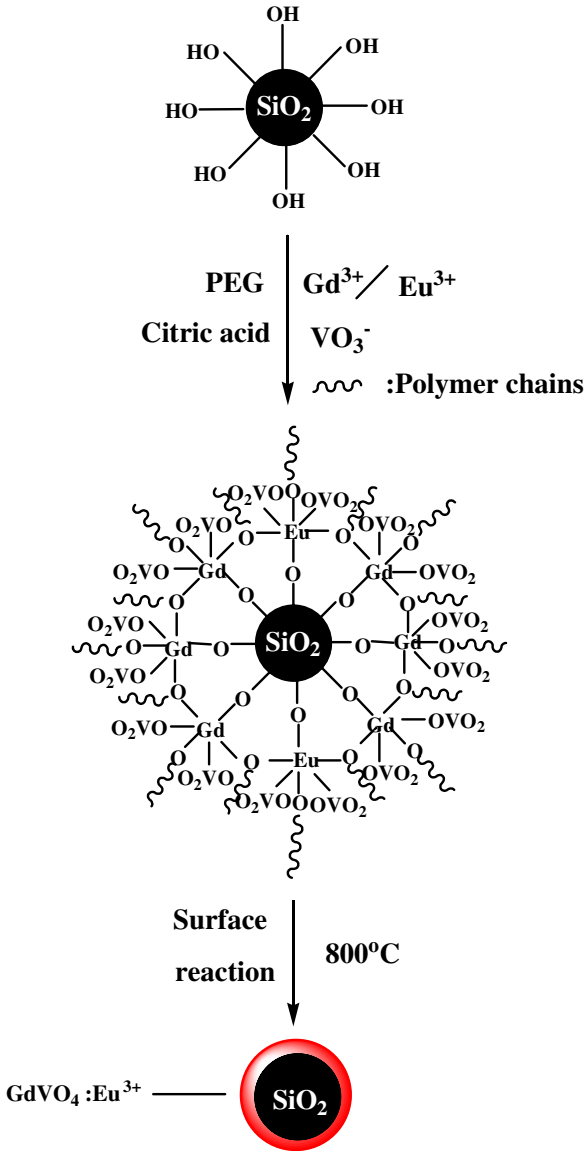

Scheme 1. Formation process of SiO_2@$GdVO_4$:Eu^{3+} core–shell particles.

powders, which were annealed in a similar process to produce the pure $GdVO_4$:Eu^{3+} powder phosphors.

2.3. Characterization

The X-ray diffraction (XRD) of the powder samples was examined on a Rigaku-Dmax 2500 diffractometer using Cu$K\alpha$ radiation ($\lambda = 0.15405$ nm). Fourier transform infrared spectroscopy (FT-IR) spectra were measured with Perkin-Elmer 580B infrared spectrophotometer with the KBr pellet technique. The morphology of the samples was inspected using a field emission scanning electron microscope (FE-SEM, XL30, Philips) and a transmission electron microscope (JEOL-2010, 200 kV). The photoluminescence (PL) and cathodoluminescence (CL) spectra were taken on a Hitachi F-4500 spectrofluorimeter equipped with a 150 W xenon lamp and 1–5 kV electron beam (self-made electron gun, 10^{-6} Pa vacuum, filament current 102.5 mA) as the excitation source, respectively. Luminescence decay curves were obtained from a Lecroy Wave Runner 6100 Digital Oscilloscope (1 GHz) using 292 nm laser (pulse width = 4 ns, gate = 50 ns) as the excitation source (Continuum Sunlite OPO). All the measurements were performed at RT.

3. Results and discussion

3.1. Formation and morphology

3.1.1. XRD

The XRD results demonstrate that the core–shell particles begin to crystallize after annealed at 600 °C. XRD patterns of as-formed fresh SiO_2 (without annealing) (a), 1000 °C-SiO_2@$Gd_{0.95}Eu_{0.05}VO_4$ (b), pure $Gd_{0.95}Eu_{0.05}VO_4$ (c) powder samples as well as the JCPDS card (No. 17-260) for $GdVO_4$ (d) are shown in Fig. 1. For SiO_2 particles (Fig. 1(a)), no diffraction peak is observed except for a broad band centered at $2\theta = 22.00°$, which is the characteristic peak for amorphous SiO_2 (JCPDS 29-0085). For the SiO_2@$Gd_{0.95}Eu_{0.05}VO_4$ core–shell sample (Fig. 1(b)), besides the broad band at $2\theta = 22.00°$ from amorphous SiO_2, all the diffraction peaks belonging to crystalline $GdVO_4$ are present, suggesting that the coatings of $Gd_{0.95}Eu_{0.05}VO_4$ have crystallized well on the surfaces of amorphous silica particles. This is in good agreement with the situation for the pure $Gd_{0.95}Eu_{0.05}VO_4$ powder sample (Fig. 1(c), in which well crystalline $GdVO_4$ is observed). No other phase is detected.

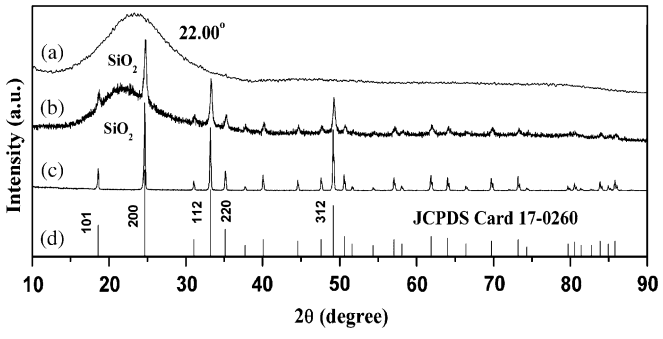

Fig. 1. X-ray diffraction patterns for as-formed fresh SiO_2 (without annealing) (a), 1000 °C-SiO_2@$Gd_{0.95}Eu_{0.05}VO_4$ core–shell particles (b), pure $Gd_{0.95}Eu_{0.05}VO_4$ powders (c) and the JCPDS card 17-260 for $GdVO_4$ (d).

3.1.2. FT-IR

The FT-IR spectra of the as-formed fresh SiO_2 (without annealing), 1000 °C-annealed SiO_2@$Gd_{0.95}Eu_{0.05}VO_4$ core–shell sample and the pure $Gd_{0.95}Eu_{0.05}VO_4$ powders are shown in Fig. 2(a)–(c), respectively. In Fig. 2(a) for the as formed SiO_2 particles, the absorption bands due to OH (3435 cm^{-1}), H_2O (1637 cm^{-1}), Si–O–Si (ν_{as}, 1100 cm^{-1}; ν_s, 803 cm^{-1}) Si–OH (ν_s, 949 cm^{-1}), and Si–O (δ, 469 cm^{-1}) bonds (where ν_{as} = asymmetric stretching, ν_s = symmetric stretching, δ = bending) are observed [27]. This indicates that the as formed SiO_2 particles contain a large amount of OH groups and H_2O on their surfaces [28]. The surface Si–OH groups play an important role for bonding the metal ions (Gd^{3+},Eu^{3+}) from the coating sol and forming the $Gd_{0.95}Eu_{0.05}VO_4$ layers on the SiO_2 surfaces in the following annealing process, as shown in Scheme 1. In Fig. 2(b) for the SiO_2@$Gd_{0.95}Eu_{0.05}VO_4$ core–shell sample, the characteristic absorption peak of V–O bond (ν_s, 825 cm^{-1}) [29], Si–O–Si bond (1103 cm^{-1}) and Si–O bond (469 cm^{-1}) for amorphous SiO_2 (Fig. 2(a)) have been observed clearly. For pure $Gd_{0.95}Eu_{0.05}VO_4$ powders (Fig. 2(c)), the strong absorption peak at 825 cm^{-1} has appeared which is attributed to the absorption of V–O bond [29]. In Fig. 2(b) and (c), the weak signal from the Gd–O bond (at 545 cm^{-1}) [30] may be covered by the strong symmetric stretching vibration of V–O bond at 825 cm^{-1}. The signal of OH groups from the as formed silica particles have almost disappeared for SiO_2@$Gd_{0.95}Eu_{0.05}VO_4$ core–shell particles annealed at 1000 °C. These results further demonstrate the formation of crystalline $Gd_{0.95}Eu_{0.05}VO_4$ coatings on the silica surfaces via the sol–gel deposition and annealing process.

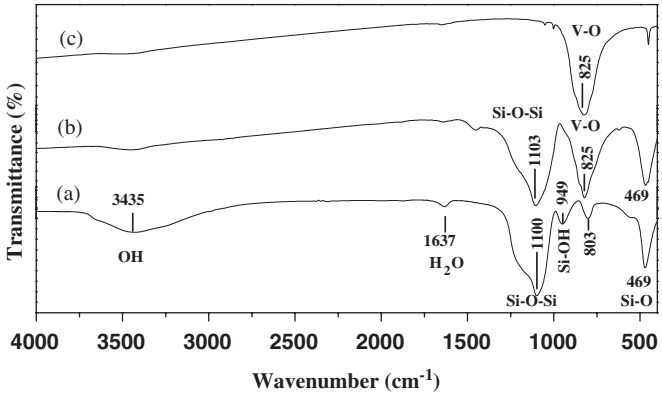

Fig. 2. FT-IR spectra of the as formed SiO_2 (without annealing) (a), 1000 °C-annealed SiO_2@$Gd_{0.95}Eu_{0.05}VO_4$ core–shell samples (b) and $Gd_{0.95}Eu_{0.05}VO_4$ powder (c).

3.1.3. FESEM and transmission electron microscopy (TEM)

Fig. 3 shows the FESEM micrographs of the as formed SiO_2 particles (a), SiO_2 particles coated by four layers of $Gd_{0.95}Eu_{0.05}VO_4$ (b) and pure $Gd_{0.95}Eu_{0.05}VO_4$ powders (c), respectively. From the FESEM micrograph of Fig. 3(a) we can observe that the as formed SiO_2 consists of spherical particles with an average size of 500 nm, and these particles are non-aggregated with narrow size distribution. After functionalizing the silica particles by $Gd_{0.95}Eu_{0.05}VO_4$ coatings, the resulted $SiO_2@Gd_{0.95}Eu_{0.05}VO_4$ particles still keep the morphological properties of the silica particles, i.e., these particles are still spherical and non-aggregated, but slightly larger than the pure silica particles due to the additional layers of $Gd_{0.95}Eu_{0.05}VO_4$ on them, as shown in Fig. 3(b). This indicates that all of the $Gd_{0.95}Eu_{0.05}VO_4$ materials have been coated on the surfaces of silica particles by our experimental process. The pure $Gd_{0.95}Eu_{0.05}VO_4$ powders contain aggregated particles, and their size is about 80–150 nm, as shown in Fig. 3(c). However, it should be mentioned that the FESEM micrographs can only provide the basic information on the morphology of $SiO_2@Gd_{0.95}Eu_{0.05}VO_4$ particles in large scale (namely, all of the SiO_2 particles remain spherical and non-aggregated subjected to the sol–gel coating of $Gd_{0.95}Eu_{0.05}VO_4$ layers on them) and the core–shell structure of $SiO_2@Gd_{0.95}Eu_{0.05}VO_4$ particles cannot be resolved from the FESEM micrographs due to the low magnification. The image of Fig. 3(d) for the energy-dispersive X-ray analysis of $SiO_2@Gd_{0.95}Eu_{0.05}VO_4$ shows that the composites are composed of Si, O, Gd, Eu and V elements.

In order to see the core–shell structure of $SiO_2@Gd_{0.95}Eu_{0.05}VO_4$ particles, TEM were performed. Representative TEM micrographs for the SiO_2 particles coated by four times (layers) of $Gd_{0.95}Eu_{0.05}VO_4$ shells as well as for the pure SiO_2 particles (as reference) are shown in Fig. 4(a) and (b), respectively. In Fig. 4(a), the core–shell structure for the $SiO_2@Gd_{0.95}Eu_{0.05}VO_4$ particles can be seen clearly due to the different electron penetrability for the cores and shells. The cores are black spheres with an average size of 500 nm (similar to the pure SiO_2 particles in Fig. 4(b)), and the shells have gray color with an average thickness of 50 nm. The electron diffraction measurement was performed in the interface region of the core and shell of a particle as labeled in Fig. 4(a), and the electron diffraction rings in Fig. 4((a), inset) demonstrate the existence of crystalline phase ($GdVO_4$) on the surface of the core–shell particles.

3.2. PL and CL properties

3.2.1. PL properties

Fig. 5 shows the excitation (a) and emission (b) spectra of $SiO_2@Gd_{0.95}Eu_{0.05}VO_4$ core–shell phosphors. The excitation spectrum was obtained by monitoring the emission of Eu^{3+} $^5D_0$–$^7F_2$ transition at 618 nm. It can be seen clearly that the excitation spectrum consists of a strong and broad band with a maximum at about 292 nm and two shoulders at 274 and 250 nm. The former can be attributed to the $GdVO_4$ host (VO_4^{3-}) excitation band, and the latter is due to the ^8S–^6I (274 nm) and ^8S–^6D (250 nm) transitions of Gd^{3+} [23]. The general *f–f* transition lines of Eu^{3+} in the longer wavelength region have not been observed due to their relatively weak intensity compared with the strong $GdVO_4$ host excitation band. The presence of the strong $GdVO_4$ host band in the excitation spectrum of Eu^{3+} indicates that there exists an efficient energy transfer from $GdVO_4$ host to the doped Eu^{3+}. Excitation into $GdVO_4$ host band at 292 nm yields the emission spectrum

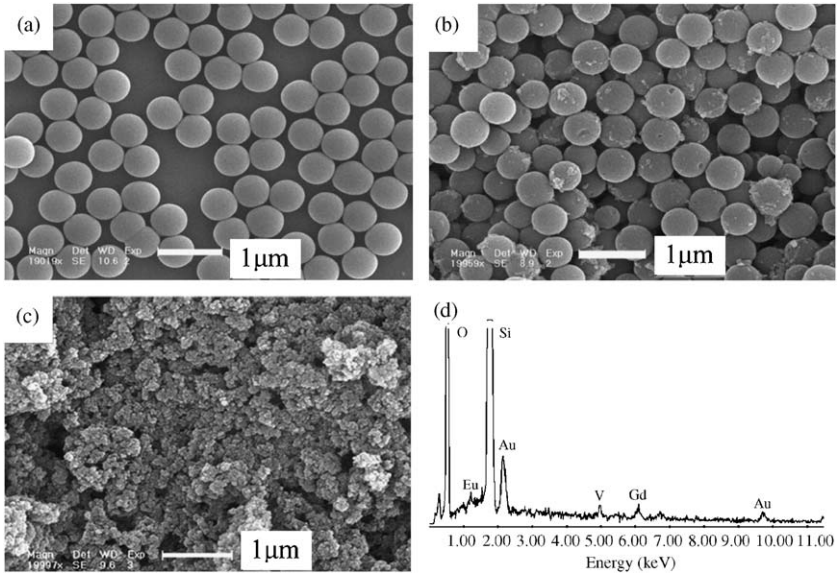

Fig. 3. SEM micrographs of the as formed SiO_2 (a), the SiO_2 particles coated with four layers of $Gd_{0.95}Eu_{0.05}VO_4$ (b), pure $Gd_{0.95}Eu_{0.05}VO_4$ powders (c) and the energy-dispersive X-ray analysis of $SiO_2@Gd_{0.95}Eu_{0.05}VO_4$ sample in (b).

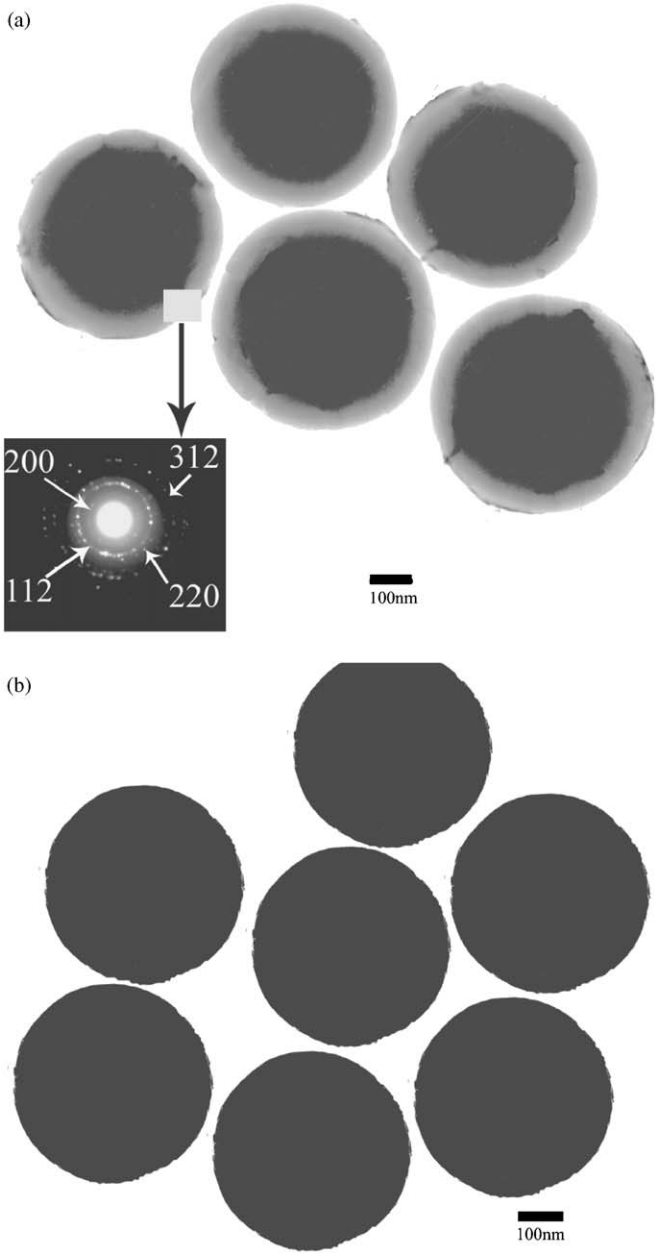

Fig. 4. TEM micrographs of the SiO_2 coated with four layers of $Gd_{0.95}Eu_{0.05}VO_4$ (a) and the bare SiO_2 particles (b). Inset: electron diffraction pattern for the selective interface region of the layers of $Gd_{0.95}Eu_{0.05}VO_4$.

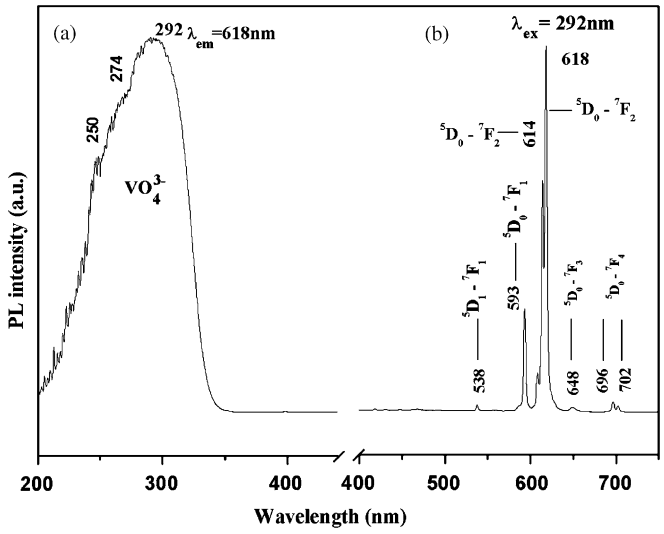

Fig. 5. Excitation (a) and emission (b) spectra of $SiO_2@Gd_{0.95}Eu_{0.05}VO_4$ core–shell particles.

corresponding to *f–f* transitions of Eu^{3+} (Fig. 5(b)), which is dominated by the hypersensitive red emission $^5D_0$–$^7F_2$ transition at 618 nm. The locations of the emission lines of Eu^{3+} and their assignments are indicated in the Fig. 5(b). Obviously, the strong emission of Eu^{3+} is due to an efficient energy transfer from the VO_4^{3-} group to Eu^{3+} in $SiO_2@Gd_{0.95}Eu_{0.05}VO_4$ core–shell particles. The $^5D_0$–$^7F_2$ emission of Eu^{3+} belongs to hypersensitive transition with $\Delta J = 2$, which is strongly influenced by outside surroundings. When the Eu^{3+} is located at a low-symmetry local site (without an inversion center), this emission transition is often dominated in the emission spectrum. This is actually the case for Eu^{3+} in the $GdVO_4$ host lattices. The crystalline $GdVO_4$ adopts the tetragonal structure with a space group of I_{41}/amd, which is composed of GdO_8 dodecahedra (the point symmetry of Gd^{3+} is D_{2d}, without an inversion center) and VO_4^{3-} tetrahedral (T_d) [31]. The Eu^{3+} ions occupy the Gd^{3+} sites in $SiO_2@GdVO_4$:Eu^{3+} core–shell particles, resulting in the hypersensitive transitions ($^5D_0$–$^7F_2$ of Eu^{3+}) being the most prominent group in the emission spectrum. In addition, the crystal field splitting of Eu^{3+} $^5D_0$–$^7F_{1,2,4}$ transitions can be seen clearly, indicating that the shell is well-crystallized. Additionally, the presence of the ^8S–^6I and ^8S–^6D absorption transitions of Gd^{3+} (Fig. 5(a)) in the excitation spectrum of $SiO_2@Gd_{0.95}Eu_{0.05}VO_4$ core–shell particles indicates that energy transfer also occurs from Gd^{3+} to Eu^{3+} besides from VO_4^{3-} to Eu^{3+} [23].

The transitions in the emission spectrum of Eu^{3+} contain those from $^5D_1$ level and $^5D_0$ level, with $^5D_1$–$^7F_1$ (prominent) and $^5D_0$–$^7F_2$ (strongest) most two representative ones, so they are chosen for luminescence decay study. The representative decay curves for the luminescence of Eu^{3+} ions in the $SiO_2@Gd_{0.95}Eu_{0.05}VO_4$ core–shell phosphors annealed at 1000 °C are shown in Fig. 6. The decay curve for $^5D_1$–$^7F_1$ (538 nm) of Eu^{3+} (Fig. 6(a)) can be well fitted into single exponential function as $I = A\exp(-t/\tau)$, (where τ is the $1/e$ lifetime of the rare-earth ion) and the fitting parameters are shown inside the Fig. 6(a). A lifetime (τ) of 5.83 μs is obtained for $^5D_1$–$^7F_1$ (538 nm) emission of Eu^{3+}. However, the decay curve for $^5D_0$–$^7F_2$ (618 nm) of Eu^{3+} (Fig. 6(b)) can be well fit into a double exponential function as $I = A_1\exp(t/\tau_1) + A_2\exp(-t/\tau_2)$, and the fitting results are shown inside the Fig. 6(b). The average lifetime for $^5D_0$–$^7F_2$ (618 nm) of Eu^{3+} is about 0.853 ms determined by the formula as $\tau = (A_1\tau_1^2 + A_2\tau_2^2)/(A_1\tau_1 + A_2\tau_2)$ [33]. The double exponential decay behavior of the activator is frequently observed when the excitation

energy is transferred from the donor [32,33]. The great difference in the lifetimes between $^5D_1$–$^7F_1$ and $^5D_0$–$^7F_2$ of Eu^{3+} can be explained as follows. The energy difference between $^5D_1$ and $^5D_0$ is 1750 cm^{-1}, which is equal to that between $^7F_3$ and $^7F_0$ of Eu^{3+} [23]. On one hand, the multiphon relaxation (non radiative transition) from $^5D_1$ and $^5D_0$ is easy to take place via the vibration of VO_4^{3-} group (phonon energy = 825 cm^{-1}, two–three phonons of VO_4^{3-} can bridge the gaps between $^5D_1$ and $^5D_0$ level of Eu^{3+}); On the other hand, the $^5D_1$ emission can also be quenched by the cross-relaxation process like $Eu^{3+}(^5D_1)+Eu^{3+}(^7F_0)\rightarrow Eu^{3+}(^5D_0)+Eu^{3+}(^7F_3)$ when the concentration of Eu^{3+} is higher than 3 mol% [23]. These factors cause the probability of nonradiative transitions from $^5D_1$ level of Eu^{3+} to be very large, thus a much shorter lifetime of the emission from $^5D_1$ level than $^5D_0$ level is resulted.

In order to further understand the energy transfer process from VO_4^{3-} to Eu^{3+} in $SiO_2@Gd_{0.95}Eu_{0.05}VO_4$,

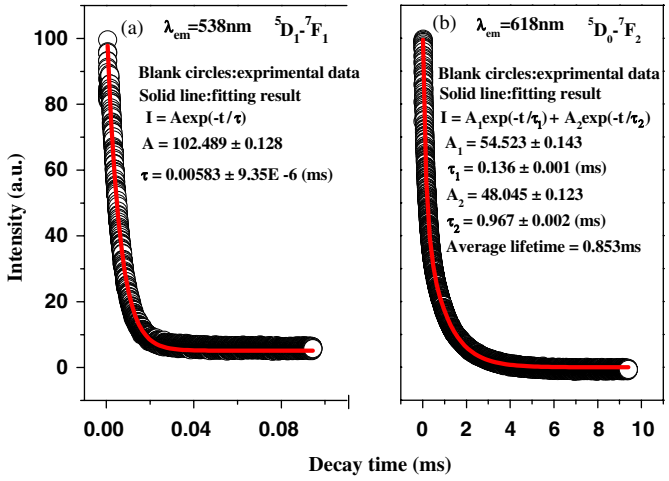

Fig. 6. The decay curves for the $^5D_1$–$^7F_1$ (538 nm) and $^5D_0$–$^7F_2$ (618 nm) emission of Eu^{3+} in $SiO_2@Gd_{0.95}Eu_{0.05}VO_4$ sample annealed at 1000 °C (λ_{ex} = 292 nm laser).

time resolved spectrum have been performed, as shown in Fig. 7. For $SiO_2@Gd_{0.95}Eu_{0.05}VO_4$, the spectra collected at different delay time exhibit characteristic line emissions from Eu^{3+}. The emission of $^5D_1$–$^7F_1$ first increased with the delay time, reaching a maximum at t = 5 μs, then began to decrease and disappeared completely at t = 50 μs. The emission of $^5D_0$–$^7F_2$ began to appear at t = 1 μs, then increased with delay time, reached the maximum at t = 50 μs and then decreased. The lifetime for the emission of $^5D_1$–$^7F_1$ (5.8 μs) is much shorter than that of $^5D_0$–$^7F_2$ (0.853 ms), so emission of $^5D_1$–$^7F_1$ at t = 5 μs began to decrease and disappeared completely at t = 50 μs.

3.2.2. CL properties

Similar to the emission under UV light excitation, the $SiO_2@Gd_{0.95}Eu_{0.05}VO_4$ core–shell particles also exhibit strong red luminescence under the excitation of electron beam. The typical emission spectra under the excitation of electron beam (1–5 kv) are shown in Fig. 8, which is basically in agreement with the PL emission spectrum (Fig. 5(b)). In the CL spectra for Eu^{3+} in $SiO_2@Gd_{0.95}Eu_{0.05}VO_4$, only the emissions from $^5D_1$–$^7F_{1,2}$ and $^5D_0$–$^7F_{1-4}$ are observed due to an efficient energy transfer from VO_4^{3-} to Eu^{3+} as well as the direct excitation of Eu^{3+} by the plasmas produced by the incident electrons. In Fig. 8, it can also be seen clearly that the CL intensity increases with the increase of accelerating voltage from 1 to 5 kV. It is known that the penetration depth of beam electrons into a particular specimen is determined by the energy of the beam electrons. The higher the energy, the greater the penetration depth. The electron penetration depth (L) can be estimated by the empirical formula: $L(\text{Å}) = 250(A/\rho)(E/Z^{1/2})^n$, where $n = 1.2/(1-0.29\log_{10} Z)$, and A is the atomic or molecular weight of the material, ρ is the density, Z is the atomic number or the number of electrons per molecule in the case compounds, and E is the anode voltage (kV) [34]. For $GdVO_4$ phosphors, the electron penetration depths at the anode voltage of 1–5 kV are estimated to be 1, 7, 23, 56 and 109 nm,

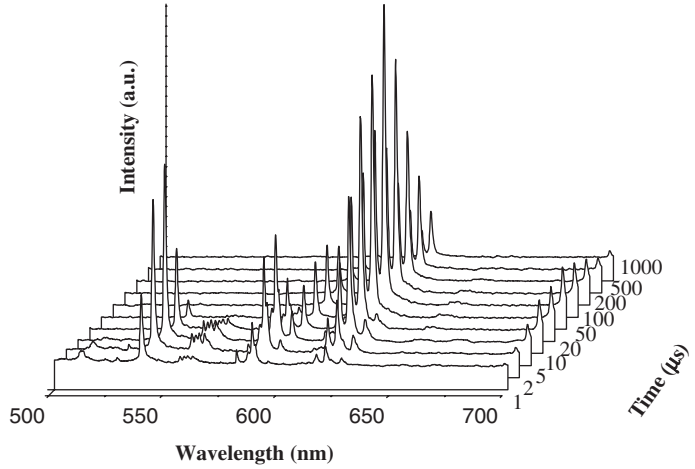

Fig. 7. Time-resolved emission spectra of Eu^{3+} in the $SiO_2@Gd_{0.95}Eu_{0.05}VO_4$ sample (λ_{ex} = 292 nm laser).

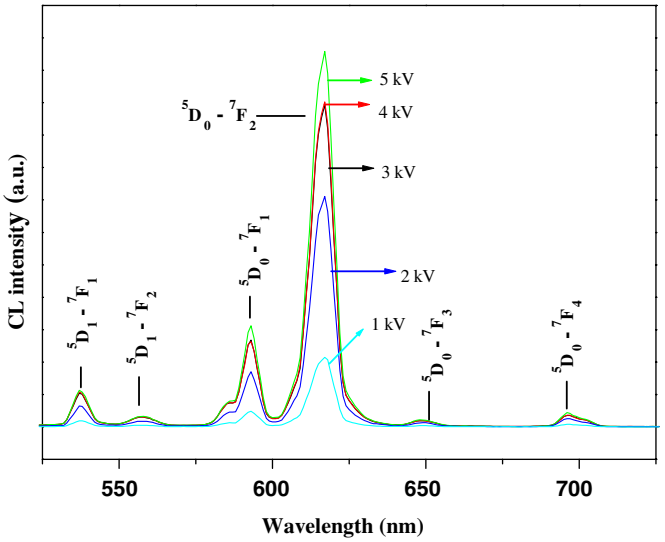

Fig. 8. CL spectra of $SiO_2@Gd_{0.95}Eu_{0.05}VO_4$ core–shell particles as a function of accelerating voltage.

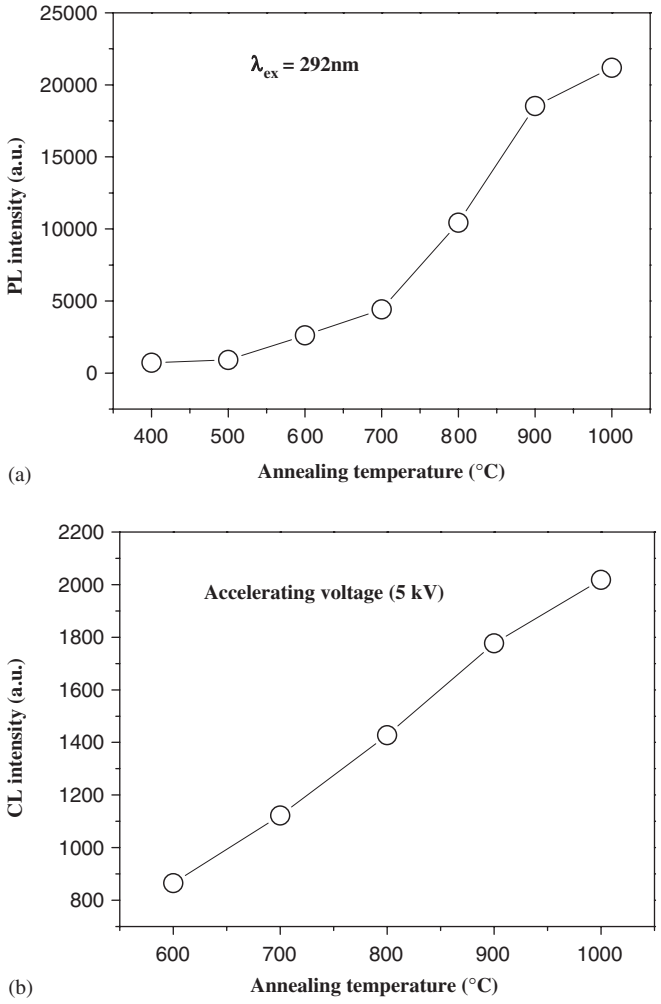

Fig. 9. The PL (a) and CL (b) emission intensities of Eu^{3+} in $SiO_2@Gd_{0.95}Eu_{0.05}VO_4$ sample as a function of annealing temperatures.

respectively. These values are within or larger than shell thickness (50 nm) of $GdVO_4$. With the increase of accelerating voltage, more plasmas will be produced by the incident electrons, resulting in more VO_4^{3-} and Eu^{3+} ions being excited and thus higher CL intensity.

3.3. Tuning of the PL and CL emission intensity

3.3.1. Temperature effects

The PL and CL emission intensities (defined as the integrated area intensities of $^5D_0$–$^7F_2$ emission peak, and this holds for all the whole following sections) of the Eu^{3+} in $SiO_2@Gd_{0.95}Eu_{0.05}VO_4$ core–shell phosphors were affected by annealing temperature. Fig. 9 shows the effect of annealing temperature on the PL and CL intensities. Both intensities increase with the increasing of annealing temperature. This is because with the increase of annealing temperature the content of impurities in the $SiO_2@Gd_{0.95}Eu_{0.05}VO_4$ core–shell phosphors such as ^-OH, NO_3^-, ^-OR, $^-CH_2$ and others decreases and the crystallinity of $Gd_{0.95}Eu_{0.05}VO_4$ shell increases. The quenching of the luminescence of the rare-earth ions by the vibrations of these impurities decreases, resulting in the increase of the emission intensity.

3.3.2. Concentration effects

By varying the content of the Eu^{3+} in $GdVO_4$ host, we determined the compositions with the highest PL emission intensity. Fig. 10 shows the dependence of the PL emission intensity of Eu^{3+} on its doping concentration (x) in $SiO_2@Gd_{(1-x)}Eu_xVO_4$ core–shell phosphors. It can be found that the PL emission intensity of Eu^{3+} increases with the increase of its concentration (x) firstly, reaching a maximum value at $x = 5$ mol%, and then decreases with increasing its content (x) due to the concentration quenching effect. Thus, the optimum concentration for Eu^{3+} is 5 mol% of Gd^{3+} in $GdVO_4$ host, which is identical with that for pure $GdVO_4$:Eu^{3+} phosphor [35].

3.3.3. Number of the coatings (N) effects

The number of the coatings (N) is also an important factor influencing PL intensity. Fig. 11(a) shows the effect of coating number on the PL intensity of $SiO_2@Gd_{0.95}Eu_{0.05}VO_4$ core–shell phosphors annealed at the same temperature. The PL intensity increases with the increasing of the coating number, which is due to the increase of the thickness of $Gd_{0.95}Eu_{0.05}VO_4$ shells on the SiO_2 spheres. When the coating number is four, the PL intensity of core–shell phosphors is about 72% of that of pure $Gd_{0.95}Eu_{0.05}VO_4$ powders excited at wavelength of 292 nm. Here it should be mentioned that the luminescent properties (e.g., PL and PLE spectra, decay lifetime) between a bulk $Gd_{0.95}Eu_{0.05}VO_4$ and core–shell structured $SiO_2@Gd_{0.95}Eu_{0.05}VO_4$ are similar except for the PL intensity discussed above. For CL, the effect of coating

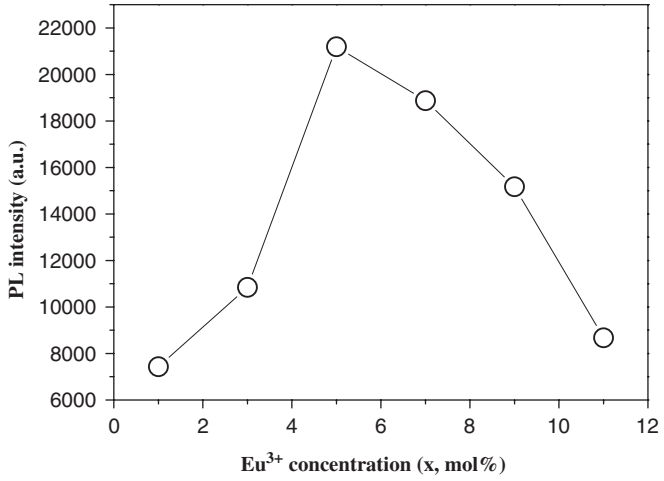

Fig. 10. The PL emission intensities of Eu^{3+} as function of its concentration (x) in $SiO_2@Gd_{(1-x)}Eu_xVO_4$ samples.

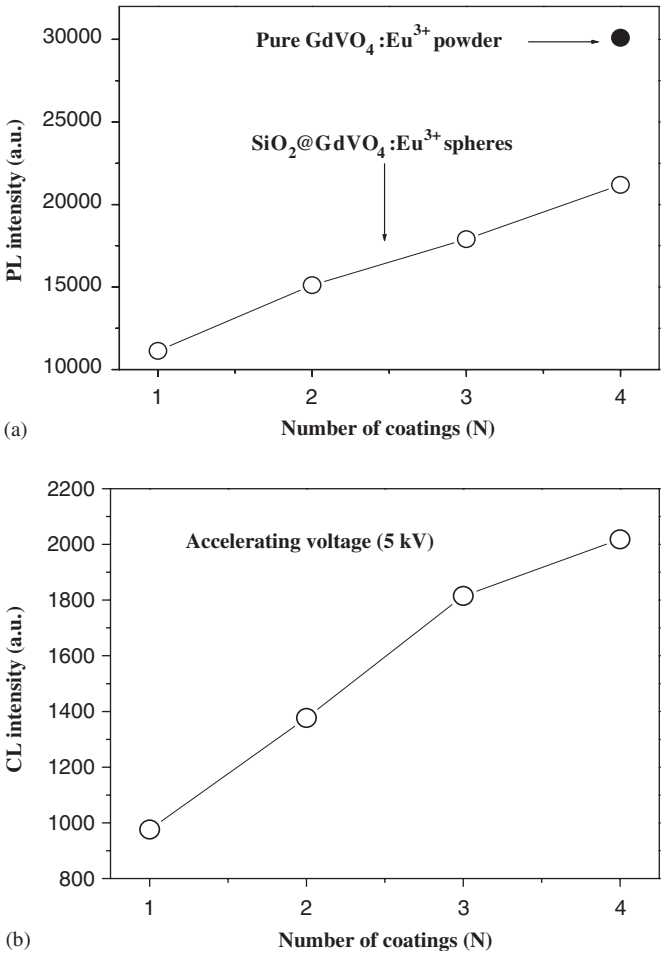

Fig. 11. The PL (a) and CL (b) emission intensities of Eu^{3+} as a function of the number of coatings (N) of $Gd_{0.95}Eu_{0.05}VO_4$ on SiO_2 particles. The PL intensity of pure $Gd_{0.95}Eu_{0.05}VO_4$ powder measured under same experimental conditions is also given for comparison.

number on its intensity of $SiO_2@Gd_{0.95}Eu_{0.05}VO_4$ core–shell phosphors is also similar to that on PL intensity, as shown in Fig. 11(b).

4. Conclusions

Submicron $SiO_2@GdVO_4:Eu^{3+}$ core–shell phosphors were successfully prepared by the sol–gel process. The obtained $SiO_2@GdVO_4:Eu^{3+}$ core–shell phosphors have spherical morphology, submicron size and narrow size distribution. The PL and CL intensities of the core–shell phosphors can be tuned by the annealing temperature and the number of coatings. With the increase of annealing temperature and the number of coatings, the PL and CL intensities increase. The optimum concentration for Eu^{3+} was determined to be 5 mol% of Gd^{3+} in $GdVO_4$ host.

Acknowledgments

This project is financially supported by the foundation of "Bairen Jihua" of Chinese Academy of Sciences, the National Natural Science Foundation of China (50225205, 50572103, 00310530, 20431030) and the MOST of China (No. 2003CB314707). Dr. M. Yu is grateful for the special starting research fund for the Awardees of President Prize of Chinese Academy of Sciences (2005–2007).

References

[1] R.A. Caruso, M. Antonietti, Chem. Mater. 13 (2001) 3272.
[2] F. Caruso, M. Spasova, V. Salgueirino-Maceira, L.M. Liz-Marzán, Adv. Mater. 13 (2001) 1090.
[3] Z.H. Jiang, C.Y. Liu, J. Phys. Chem. B 107 (2003) 12411.
[4] H. Sertchook, D. Avnir, Chem. Mater. 15 (2003) 1690.
[5] P. Mulvaney, M. Giersig, T. Ung, L.M. Liz-Marzán, Adv. Mater. 9 (1997) 570.
[6] T. Ung, L.M. Liz-Marzán, P. Mulvaney, Langmuir 14 (1998) 3740.
[7] S.J. Oldenburg, R.D. Averitt, S.L. Westcott, N.J. Halas, Chem. Phys. Lett. 288 (1998) 243.
[8] M.S. Fleming, T.K. Mandal, D.R. Walt, Chem. Mater. 13 (2001) 2210.
[9] H. -L. Xia, F. -Q. Tang, J. Phys. Chem. B 107 (2003) 9175.
[10] P. Schuetzand, F. Caruso, Chem. Mater. 14 (2002) 4509.
[11] S.R. Hall, S.A. Davis, S. Mann, Langmuir 16 (2000) 1454.
[12] I. Sondi, T.H. Fedynyshyn, R. Sinta, E. Matijevic, Langmuir 16 (2000) 9031.
[13] H. Wang, C.K. Lin, X.M. Liu, J. Lin, Appl. Phys. Lett. 187 (2005) 181907.
[14] G.X. Liu, G.Y. Hong, J. Colloid Interface Sci. 278 (2004) 133.
[15] M. Yu, J. Lin, J. Fang, Chem. Mater. 17 (2005) 1783.
[16] D.Y. Kong, M. Yu, C.K. Lin, X.M. Liu, J. Lin, J. Fang, J. Electrochem. Soc. 152 (9) (2005) H146.
[17] W. Stöber, A. Fink, E. Bohn, J. Colloid Interface Sci. 26 (1968) 62.
[18] P.A. Studenikin, A.I. Zagumennyi, Y.D. Zavartsev, P.A. Popov, I.A. Shcherbakov, Quantum Electron. 25 (1995) 1162.
[19] A.I. Zagumennyi, Y.D. Zavartsev, P.A. Studenikin, I.A. Scherbakov, F. Umyskov, P.A. Popv, V.B. Ufimtsev, Proc. SPIE Int. Soc. Opt. Eng. 2698 (1996) 182.
[20] V.A. Mikhailov, Y.D. Zavartsev, A.I. Zagumennyi, Quantum Electron. 27 (1997) 13.
[21] E. Antic-Fidancev, M. Lemaître-Blaise, Spectrochim. Acta Part A 54 (1998) 2151.
[22] F.C. Palilla, A.K. Levin, M. Rinkevics, J. Electrochem. Soc. 122 (1965) 776.
[23] G. Blasse, B.C. Grabmeter, Luminescent Materials, Springer, Berlin, 1994.

[24] A.M. Pires, M.R. Davolos, E.B. Stucchi, Int. J. Inorg. Mater. 3 (2001) 785.
[25] M.P. Pechini, US Patent No. 3330 697, 1967.
[26] M. Yu, J. Lin, J. Fu, H.J. Zhang, Y.C. Han, J. Mater. Chem. 13 (2003) 1413.
[27] A. Kioul, L. Mascia, J. Non-Cryst. Solids 175 (1994) 169.
[28] S.J. Oldenburg, R.D. Averitt, S.L. Westcott, N.J. Halas, Chem. Phys. Lett. 288 (1998) 243.
[29] N. Weinstock, H. Schulze, A. Muller, J. Chem. Phys. 59 (1973) 5063.
[30] A. García-Murillo, C.L. Luyer, C. Dujardin, C. Pedrini, J. Mugnier, Opt. Mater. 16 (2001) 39.
[31] C. Hsu, R.C. Poweh, J. Lumin. 10 (1975) 273.
[32] S. Mukarami, H. Markus, R. Doris, M. Makato, Inorg. Chim. Acta 300–302 (2000) 1014.
[33] K. Riwotzki, H. Meyssamy, A. Kornowski, M. Haase, J. Phys. Chem. B 104 (2000) 2824.
[34] C. Feldman, Phys. Rev. 117 (1960) 455.
[35] B.N. Mahalley, R.B. Pode, P.K. Gupta, Phys. Stat. Sol. (a) 177 (1999) 293.